International Journal of Nanomedicine

Dovepress

open access to scientific and medical research

Open Access Full Text Article

ORIGINAL RESEARCH

Superior Drug Delivery Performance of Multifunctional Bilosomes: Innovative Strategy to Kill Skin Cancer Cells for Nanomedicine Application

Ewelina Waglewska[1], Julita Kulbacka[2,3], Urszula Bazylinska[1]

[1]Department of Physical and Quantum Chemistry, Faculty of Chemistry, Wroclaw University of Science and Technology, Wroclaw, Poland; [2]Department of Molecular and Cellular Biology, Faculty of Pharmacy, Wroclaw Medical University, Wroclaw, Poland; [3]State Research Institute Centre for Innovative Medicine, Department of Immunology and Bioelectrochemistry, Vilnius, Lithuania

Correspondence: Urszula Bazylinska, Department of Physical and Quantum Chemistry, Faculty of Chemistry, Wroclaw University of Science and Technology, Wybrzeze Wyspianskiego 27, Wroclaw, 50-370, Poland, Tel +48 713202183, Email urszula.bazylinska@pwr.edu.pl

Purpose: Numerous failures in melanoma treatment as a highly aggressive form of skin cancer with an unfavorable prognosis and excessive resistance to conventional therapies are prompting an urgent search for more effective therapeutic tools. Consequently, to increase the treatment efficiency and to reduce the side effects of traditional administration ways, herein, it has become crucial to combine photodynamic therapy as a promising therapeutic approach with the selectivity and biocompatibility of a novel colloidal transdermal nanoplatform for effective delivery of hybrid cargo with synergistic effects on melanoma cells.

Methods: The self-assembled bilosomes, co-stabilized with L-α-phosphatidylcholine, sodium cholate, Pluronic® P123, and cholesterol, were designated, and the stability of colloidal vesicles was studied using dynamic and electrophoretic light scattering, also provided in cell culture medium (Dulbecco's Modified Eagle's Medium). The hybrid compounds – a classical photosensitizer (Methylene Blue) along with a complementary natural polyphenolic agent (curcumin), were successfully co-loaded, as confirmed by UV-Vis, ATR-FTIR, and fluorescent spectroscopies. The biocompatibility and usefulness of the polymer functionalized bilosome with loaded double cargo were demonstrated in vitro cyto- and phototoxicity experiments using normal keratinocytes and melanoma cancer cells.

Results: The in vitro bioimaging and immunofluorescence study upon human skin epithelial (A375) and malignant (Me45) melanoma cell lines established the protective effect of the PEGylated bilosome surface. This effect was confirmed in cytotoxicity experiments, also determined on human cutaneous (HaCaT) keratinocytes. The flow cytometry experiments indicated the enhanced uptake of the encapsulated hybrid cargo compared to the non-loaded MB and CUR molecules, as well as a selectivity of the obtained nanocarriers upon tumor cell lines. The phyto-photodynamic action provided 24h-post irradiation revealed a more significant influence of the nanoplatform on Me45 cells in contrast to the A375 cell line, causing the cell viability rate below 20% of the control.

Conclusion: As a result, we established an innovative and effective strategy for potential metastatic melanoma treatment through the synergism of phyto-photodynamic therapy and novel bilosomal-origin nanophotosensitizers.

Keywords: nanovesicular carriers, human melanoma, A375 cells, Me45 cells, antitumor activity, phyto-photodynamic therapy

Introduction

The level of cancer incidence has dramatically increased over recent years. Prominent among them is malignant melanoma, diagnosed each year in about 1.7% of primary malignancies and contributing to 0.7% of cancer-related deaths.[1] Melanocyte-derived melanoma, usually found in the innermost part of the epidermis (basal layer), is the most malignant type of skin cancer due to its rapid growth rate and numerous metastases. It can spread to various body parts, from draining lymph nodes to distant visceral organs, especially the brain, lungs, bones, and liver. In addition to surgical

Received: 6 December 2023
Accepted: 19 April 2024
Published: 23 May 2024

Graphical Abstract

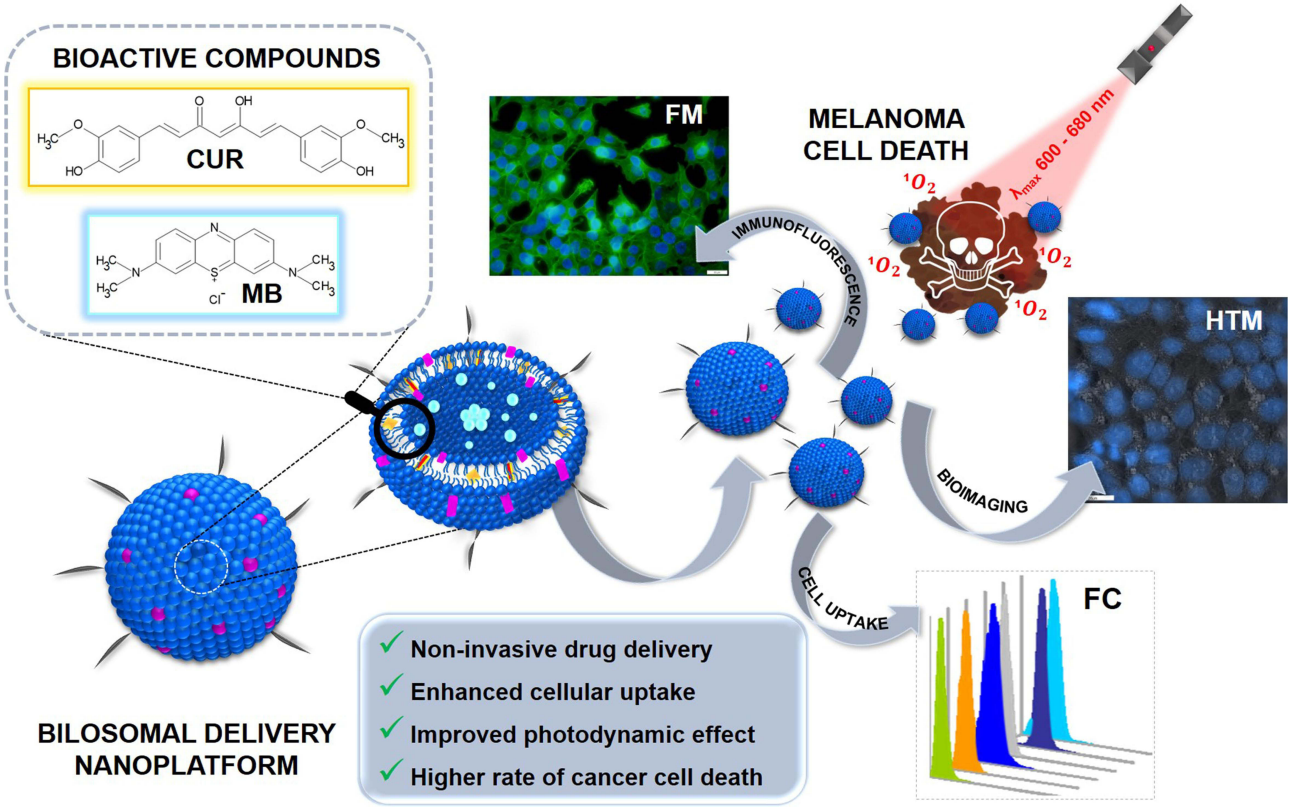

resection, standard clinical treatments include chemotherapy, radiation therapy, and immunotherapy. Targeted therapy based on gene editing tools, among other approaches, has also received tremendous attention in the field of melanoma treatment.[2,3] However, the inherent resistance of melanoma to traditional methods (especially for metastatic forms) is a severe concern for modern oncology, which motivates scientists to develop emerging strategies to fight melanoma.[4–6]

Due to its high degree of efficacy, safety of use, and non-invasiveness, photodynamic therapy (PDT) is a therapeutic approach that has attracted considerable interest among researchers for many cancer treatments. PDT is now FDA-approved as one of the methods officially used to treat basal cell and squamous cell carcinoma (a group of cancers developing in the upper layers of the skin), as well as certain types of esophageal and lung cancers by the US Food and Drug Administration (FDA). In recent years, research has also been conducted on the application of PDT for patients with head, neck, breast, and melanoma cancers.[7] Unlike conventional therapeutic options, PDT limits damage to healthy cells and has high selectivity and minimal systemic side effects.[8,9] The action of PDT is based on a phototoxic reaction by combining photosensitizing agents and laser radiation at a specific wavelength to generate reactive oxygen species (ROS) that are fatal to cancer cells. It can induce tumor cell necrosis, tumor blood vessel damage, and immunogenic tumor cell death, activating the immune response against cancer and thus indicating significant prospects for clinical application.[10,11] However, for malignancies with high metastatic potential, such as melanoma, the application of PDT therapy is hampered by, among other things, the presence of a variety of defense mechanisms (including anti-apoptotic) and escape pathways from metastatic treatment. In addition, the high level of naturally occurring pigment in the skin (melanin) may act as an optical shield (500–600 nm spectral region) and as an antioxidant that competes with the photosensitizers (PSs) used for photons, thus reducing the efficiency of their photoreaction, which may ultimately lead to a reduction in the effectiveness of PDT in treating this cancer.[12] As a result, researchers continue to look for new opportunities to improve the efficacy of PDT in treating melanoma, thus devoting increasing attention to combinatorial anticancer therapy (ie, the use of two or more active compounds), which shows superior therapeutic benefit compared to monotherapy. Therefore, its

primary goal is to act synergistically due to the different biological mechanisms of the drugs and minimize side effects through multidirectional effects on tumors.[13,14]

In recent years, research has intensified on bioactive compounds derived from plants, which may play a significant role in treating malignant melanoma due to their multiple mechanisms of action. They are increasingly considered complementary chemopreventive agents with anti-cancer or anti-inflammatory effects that can reverse, inhibit, or prevent cancer development.[15] Importantly, these naturally occurring compounds can act synergistically in combination with classical photosensitizers used in PDT therapy by increasing the rate of tumor cell apoptosis, enhancing the ability to generate ROS, or effectively inhibiting cell proliferation through photoinductive effects.[16] Recent studies have shown that curcumin is one of the crucial phytopharmaceuticals in melanoma treatment. Among other things, it can exert anti-melanoma effects by activating apoptosis and preventing angiogenesis and metastasis (including lungs), alongside contributing to the epithelial-mesenchymal transition's (EMT) inhibition and affecting melanoma progression through factors such as mitogen-activated protein kinase (MAPK), microRNA, p21 and Bcl2, among others. However, it should be underlined that the clinical use of many active compounds in their free (non-encapsulated) form is limited due to the poor therapeutic index resulting from their low bioavailability, poor water solubility, possible degradation under the influence of various factors (ie, temperature, light, pH) or rapid clearance of the drug.[17,18]

Nanotechnology offers countless opportunities to improve the physicochemical properties of phytotherapeutics and photosensitizers used in photodynamic therapy, as well as the ability to deliver them simultaneously by, among other things, encapsulating them in innovative self-assembling colloidal nanostructures with high biocompatibility and biodegradability. The action of standard combination therapy can be restricted by the different pharmacokinetics of the therapeutic agents, which often results in uncoordinated uptake of the various active compounds by the cancer cell, thereby reducing their synergistic anti-tumor effects.[19] Therefore, they offer several advantages for combinatorial drug delivery in terms of, among other things, selective accumulation in the tumor microenvironment through enhanced permeability and retention (EPR) effects, thus promoting synergistic action of therapeutic agents at the target site.[20]

Based on our previous extensive studies, the nanoplatform we synthesized for transdermal delivery demonstrated the combined therapeutic effect of a bilosomal carrier encapsulating a classical photosensitizer in an aqueous core (Methylene Blue, MB) along with a complementary natural compound (curcumin, CUR) in the bilosome's lipid bilayer, thereby achieving high antimicrobial activity.[21,22] The overall concept of our studies is presented in Scheme 1. Accordingly, the present work

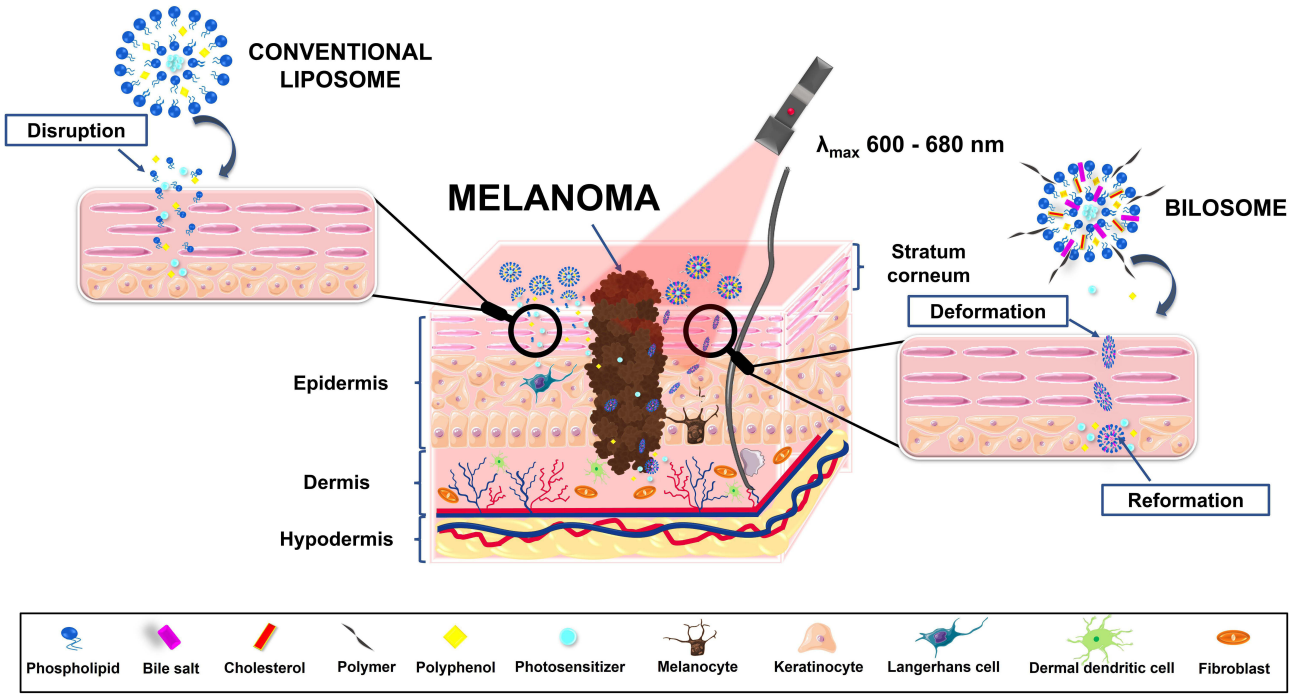

Scheme 1 Comparison of the skin permeation mechanisms of the proposed functional bilosomes over conventional liposomes, with particular emphasis on their potential application in melanoma treatment.

further extends the use of the nanoplatform we developed to demonstrate its complete versatility in various skin applications. The primary goal of this research was to perform biological stability followed by bioimaging and immunofluorescence study using holotomographic microscopy (HTM) and fluorescence microscopy (FM), as well as to evaluate the cytocompatibility and phyto-photodynamic activity of the developed nanosystems against both normal human epidermal keratinocytes and skin melanoma cell lines: human epithelial skin melanoma cells (A375) and human malignant melanoma Me45 cell line. The bilosomal nanostructure we developed and its subsequent application to enhance the photodynamic treatment of melanoma, including its comparison with the effects of the free photosensitizer, is an incredibly novel therapeutic approach for this type of skin cancer that has not been reported before. We anticipate that the results obtained in this work will provide further inspiration for the development of self-assembling pharmaceutical nanosystems technology to co-encapsulate two bioactive compounds with synergistic effects for carrier-enhanced anti-tumor activity, which may ultimately contribute towards the effective use of the innovative phyto-photodynamic therapy (phyto-PDT) as a supplementary treatment for patients suffering from malignant melanoma.

Experimental Section

Materials

The following chemical compounds, acquired from Sigma-Aldrich (Poznan, Poland), were used to formulate the functional bilosomes: L-α-Phosphatidylcholine (PC, egg yolk), sodium cholate hydrate (SC, ≥97%), Pluronic®P-123 (PP123, Mn ~5800), and curcumin (CUR). Methylene Blue (MB, 1% solution of injection) was manufactured by Akorn, Inc. (Lake Forest, IL 60045, USA). Cholesterol (Chol) was purchased from CRODA Inc. (East Yorkshire, England). The necessary solvents, including chloroform ($CHCl_3$) and tetrahydrofuran (THF), were obtained from Avantor Performance Materials Poland SA - Gliwice. Other chemical reagents were used as received from commercial producers. The distilled water used in our analysis was prepared by the HLP Smarty Hydrolab system (Labsystem S.C., Kraków, Poland).

General Procedure for the Preparation of Pluronic®P123-Modified Nanoplatform

The preparation of double-loaded Pluronic®P123-stabilized bilosomes containing PC, Chol, and SC by thin-film hydration technique (known as the Bangham method) was outlined in our previous investigation.[21] In short, a mixture of lipids, triblock copolymer, and curcumin was dissolved in 2 mL of $CHCl_3$ at a total concentration of 10 mg/mL PC, 3 mg/mL Chol, 6 mg/mL PP123, and 0.05 mg/mL CUR respectively, and mixed by slightly shaking of a 10 mL round bottom flask. In the next step, the organic solvent was removed using a Heidolph Hei-VAP Value Digital Rotary Evaporator (Schwabach, Germany) at 40 °C. The thin lipid film (formed on the flask's wall) was rehydrated using an aqueous medium: distilled water with SC (5 mg/mL) and MB (0.05 mg/mL). The resulting dispersion was then stirred on the magnetic stirrer, and finally, small unilamellar vesicles (SUVs) with uniform size were produced by ultrasonic bath sonication. For comparison, blank vesicles (without active cargo) were also prepared. After preparation, the obtained samples were kept in the fridge (4 °C) for subsequent experiments.

Characterization of Nanovesicles Colloidal Properties

Particle Size Distribution and Zeta Potential Measurements

The particle size of bilosomes (blank and MB/CUR-co-loaded) was specified by measuring Brownian motions of nanoparticles using dynamic light scattering (DLS) technique by Zetasizer Nano Series from Malvern Instruments (Worcestershire, UK; DTS software) with an angle of incidence of light equal to 173°. Three runs with at least ten measurements in disposable polystyrene cuvettes were performed at 25 °C and were reported as Z-average (Z-Ave) in conjunction with polydispersity index (PdI). The nanobilosomes' surface electric charge (ζ-potential) was determined using the Smoluchowski equation, using the electrophoretic mobility technique and monitoring the movement of the particles in an electric field. The measurements were conducted in a folded capillary zeta cell at 25 °C using the same apparatus as above (three consecutive instrument runs, with at least twenty measurements). Z-Ave, PdI, and ζ-potential measurements were performed again after a suitable incubation time (14 and 30 days) at 4 °C to check the system's stability.

Shape and Morphological Assessments

The morphological characteristics of the functional nanoplatform were identified through the FEI Tecnai G2 20 X-TWIN transmission electron microscope (TEM, Hillsboro, OR, USA) after 10-fold dilutions. One drop of the MB/CUR-bilosomes dispersion (around 10 μL) was adsorbed on the carbon-coated support copper TEM grid and subsequently air-dried for 1 hour at room temperature prior to TEM observations.

Evaluation of the Encapsulation Efficiency of Active Compounds Using UV-Vis and ATR-FTIR Spectroscopy

The Hitachi's U-5100 UV-visible spectrophotometer (Mannheim, Germany) was applied to determine the Methylene Blue and curcumin encapsulation efficiency (EE) in the Pluronic®P123-stabilized bilosome formulation. Before the appropriate measurements, the dispersion was purified from the non-encapsulated active substances using dialysis bags acquired from Carl Roth (cut-off: 14,000 Da, Germany). The functional bilosomes were disrupted with a mixture of THF and H_2O (1:1), followed by target UV-Vis measurements (quartz cuvette with 1 cm path length). Absorption maxima were read at 666 nm for Methylene Blue and 426 nm for curcumin. Finally, EE was calculated as follows: EE=(amount of pharmaceutical drug encapsulated in vesicles/total amount of pharmaceutical drug added) × 100%.

To verify the effectiveness of co-encapsulation of the active compounds in the bilosomes, we also used an attenuated total reflection-Fourier transform infrared spectroscopy (ATR-FTIR). Blank, as well as co-loaded bilosome formulations, were lyophilized before the target measurements for 48 hours. Then, possible interactions between the cargo and the nanocarrier were investigated, with the use of Bruker's Vertex 70 v vacuum spectrophotometer (Billerica, MA, USA) fitted with an air-cooled DTGS detector and diamond attenuated total reflection accessory. All spectra were observed in the range of 4000–400 cm^{-1} (4 cm^{-1} resolution), accumulating 128 scans for each sample at 25 °C. The collected spectra of MB/CUR-co-loaded bilosomes were compared with pure MB, pure CUR, and blank Pluronic®P123-stabilized bilosomes.

Fluorescence Spectroscopic Studies

Fluorescence spectra of the hydrophilic photosensitizer were measured in pure form and after MB encapsulation in functional bilosomes to determine possible changes in fluorescence emission after its encapsulation in the nanostructure. Fluorescence measurements were carried out on a Spectrofluorometer FS5 (Edinburgh Instruments Ltd., Livingston, UK) in the range of 670–800 nm at the excitation wavelength of 666 nm.

Biological Stability

Studies to measure biological stability against aggregation of functional bilosomes (evaluation of the Pluronic "stealth" effect), as well as possible proteins adsorption, were carried out in Dulbecco's Modified Eagle's Medium (DMEM, cell standard medium acquired from Sigma-Aldrich, Poznan, Poland) without or with 10% fetal bovine serum (FBS, BioWhittaker) and antibiotics (penicillin/streptomycin, Sigma-Aldrich, Poznan, Poland), in a humidified atmosphere that contains 5% CO_2 at 37 °C. Measurements of the system's size (Z-Ave including PdI) were performed in seven various periods of time (from 0–168 hours) with a ratio of nanocarrier suspension to culture medium – 1:4.

In vitro Biological Response Upon Melanoma Cells

Human Cell Lines

In vitro studies were conducted on human melanoma cells derived from a 54-year-old woman patient (A375) and malignant melanoma cells derived from cutaneous melanoma metastasis to lymph nodes (Me45). Primary human epidermal keratinocytes (HaCaT) were used as the normal cell line. A375 and HaCaT cells were purchased from ATCC® (LGC Standards, Poland). The Me45 cell line was received from the Oncology Centre in Gliwice (Poland), where it was taken from the lymph node cells of a 35-year-old female patient. The cells thus obtained were maintained in culture flasks with a surface area equal to 75 cm^2 (Falcon® Cell Culture Flasks) in basal medium for supporting cell growth (DMEM, IITD, Wroclaw, Poland) supplemented with 10% fetal bovine serum (FBS) and 50 μg/mL penicillin and streptomycin (Sigma-Aldrich, Poznan, Poland). The cultures were incubated in a humidified atmosphere with 5% CO_2 at 37 °C (optimal temperature conditions needed for cell growth). The cells destined for all experiments were detached by

trypsinization (Trypsin-EDTA solution), neutralized with complete cell culture medium (DMEM with FBS), and devoted to further analysis.

Flow Cytometry Uptake Analysis of the Encapsulated Hybrid Cargo

Flow cytometry analysis was performed to assess the ability to internalize and uptake free and enveloped MB and CUR in the melanoma (A375, Me45) and normal HaCaT cells. Cells were detached with Trypsin–EDTA and exposed to free and encapsulated MB and CUR. Bilosomes were added with a final MB concentration equal to 1 and 2 μM, and cells were incubated for 24 h at 37 °C in a humidified atmosphere containing 5% CO_2. Then, cells were trypsinized, washed in PBS, and resuspended in 0.5 mL of PBS. Flow cytometric analysis was conducted on a CyFlow Cube 6 flow cytometer (Sysmex, Poland). The fluorescence of MB with CUR was measured with an FL-3-H detector (exc: 488 nm, em: 700±50 nm). Samples were analyzed in minimum triplicate repetition; 10^4 cells/sample was measured each time. Data were collected and analyzed using CyView software (Sysmex, Poland).

Immunofluorescent F-Actin Staining Protocol and Cell Morphology

Cancer cells were seeded directly on 18 mm diameter round microscope coverslips (Thermo Fisher Scientific Inc.) in 6-well plates (Sarstedt, EquiMed, Poland). The cells were left to adhere for 24 hours. After this time, the cells were treated with bilosomes for 24 hours. The cells were washed twice with phosphate-buffered saline (PBS, BioShop, EPRO, Poland), fixed for 10 minutes in 4% paraformaldehyde (Polysciences, Inc., Bergstrasse, Germany), and washed again with PBS. The cytoskeleton was determined by immunofluorescent labeling of F-actin cells with Alexa Fluor®546 Phalloidin (Thermo Fisher Scientific Inc.). Fluorshield™ with a fluorescent DNA-binding dye of cells grown in the culture (4,6-diamidino-2-phenylindole, DAPI) was used to visualize the nuclei and mount the cells after excitation at 405 nm. Samples were examined on an Olympus BX53 fluorescence microscope (Evident Europe GmbH, Warsaw, Poland). For cell morphology, analysis of the 3D Cell Explorer holotomographic microscope (HTM) was used (Nanolive SA, Sygnis, Poland). Images of the samples were taken and analyzed using Steve software (Nanolive SA, Sygnis, Poland).

In vitro Red-Light-Induced Anticancer Activity

For cytotoxicity and photocytotoxicity evaluation, the cell lines tested cell lines were placed at 200 μL each per well (density of approximately 2×10^4 cells) into 96-well plates (Sarstedt, EquiMed, Wroclaw, Poland). The in vitro antitumor activity of the tested bilosomes containing MB and CUR (in the concentration range for Methylene Blue from 0.5 μM to 12.5 μM after dilution in the culture medium) was examined using the MTT (3-(4,5-dimethylthiazol-2-yl)-2,5-diphenyl tetrazolium bromide) cell proliferation assay (Sigma-Aldrich, Poznan, Poland). Cytotoxicity experiments were performed after 24 and 72 h incubation with bilosomes. For photocytotoxicity experiments, the cells were incubated with bilosomes or drugs for 4 hours. After this time, the cells were irradiated for ten minutes with a total light dose of 10 J/cm^2 using an OPTEL Fibre Illuminator (Opole, Poland) equipped with polarized light filtered with barrier filters (λ_{max} 600–680 nm). At the level of the cell monolayer, the energy fluency ratio was 12 mW/cm^2. Irradiation dose was verified each time by the light intensity meter for the appropriate wavelength (Optel). The MTT assay was used to examine the effectiveness of PDT 24 hours after the incubation. Cell viability in each test group was expressed as percentages of the control cells (untreated with studied bilosomes). Then, the absorbance was measured at 560 nm using a GloMax® Discover Microplate Reader (Promega). The final results shown in the graphs were subtracted from the blank and normalized to the untreated control. All experiments in this study were conducted in triplicate, which gave us accurate and precise measurement results.

Results and Discussion

Physicochemical Characterization of Bilosomal Delivery Nanoplatform

Recent studies show that the most common method of photosensitizer delivery in PDT is an intravenous injection and oral administration.[23] However, these routes of PSs administration can pose serious problems related to the insufficient accumulation of the drug, its distribution in many other organs, and the degradation of PSs in the gastrointestinal tract (GIT). An outstanding alternative to intravenous and also oral delivery of bioactive agents can be topical/transdermal application, which has great potential in the treatment of many diseases, including skin diseases. Its therapeutic benefits are primarily related to the possibility of non-invasively delivering pharmaceuticals with minimized pain and risk of

infection, reducing systemic toxicity, avoiding first-pass metabolism by the liver, avoiding strongly acidic pH in the stomach, and avoiding possible enzymatic degradation of drugs in the GIT.[4,24]

Transdermal delivery of active compounds is restricted by the outermost layer of human skin (*stratum corneum*), which is the so-called "epidermal wall" since this layer consists of closely adherent cells (corneocytes) surrounded by a lipid-rich intercellular matrix.[25] One of the most popular nanosystems for transdermal drug delivery is liposomes (renowned as vesicle carriers). They consist primarily of phospholipids, which have a high degree of biocompatibility and biodegradability, guaranteeing maximum safety for the body. However, due to the lack of deformability of these conventional carriers, they are prone to tearing, so their use is constrained to the epidermal surface only.[26] Thus, the recent focus has been on developing new generations of modified vesicle nanocarriers, which would make it possible to improve the permeability of active ingredients to deeper levels of the skin. Among other things, we can include bilosomal carriers, whose structure is based on non-ionic surfactants (including polyoxyethylene synthetic compounds with the trade names Tween®80 or Span®80), cholesterol, and bile salt molecules.[27] The addition of a non-ionic surfactant as an "edge activator" helps lower the interfacial tension, resulting in vesicle deformation. However, these synthetic emulgators have low biodegradability, as well as high sensitivity to environmental factors (pH, temperature), while causing skin irritation. Therefore, to improve biocompatibility, as well as reduce potential side effects, our proposed "smart" carriers use highly biodegradable and non-toxic phospholipids (that is phosphatidylcholine (PC), which is the main component of cell membranes), cholesterol (Chol) as an auxiliary lipid, and biosurfactant reagent (bile salt) as an agent to increase their penetration through the skin by interacting with phospholipids in cell membranes (sodium cholate, SC). In addition, we increased the bilosome surface's stability by adding a biocompatible triblock copolymer (Pluronic P123, PP123), which forms a specific steric barrier in the form of outer hydrophilic poly (ethylene oxide) groups around the carrier structure. The main differences in the interaction of the nanocarriers (conventional liposomes and bilosomes) with the skin are shown in Scheme 1.

The physicochemical properties determine the biological identity of the developed nanocarriers, thus influencing their in vivo transport, biological distribution, or cellular uptake. Ultimately, they also determine the fate of the active compounds encapsulated in them.[28] The particle size (Z-Average size, Z-Ave), size distribution range (polydispersity index, PdI), and surface charge ratio (zeta potential, ζ-potential) of empty bilosomes and double-loaded bilosomes (MB+CUR) were assessed by DLS and ELS (Figure 1A and C). As can be seen, the vesicle size (from 83 nm to 98 nm) and PdI values (0.254 and 0.267) are little affected by the presence of an active cargo. Overall vesicle sizes in the 50–200 nm range and PdI values less than 0.3 are highly favorable for vesicular drug carriers in clinical development. In addition, small vesicles (less than 100 nm) can significantly permeate the *stratum corneum* between corneocytes in the *stratum corneum* (via the intercellular pathway), thereby increasing the uptake of encapsulated drugs in the epidermis as well as the dermis, which is particularly important for transdermal administration.[29] Uniform spherical bilosomal nanostructures and a narrow size distribution for the double-loaded formulation (MB/CUR-bilosomes) were confirmed by TEM (Figure 1B). The ζ-potential of the developed bilosomes was also investigated, which is an important parameter that verifies the nanocarrier's stability and thus affects its further fate in the human body. High repulsive electrostatic forces on the bilosome surface (with highly negatively charged in the range of −37 to −31 mV) contributed to their significant colloidal stability, which was confirmed in a stability test (Figure 1C), in which we observed no significant change in zeta-potential values after storing (for 30 days) in the dark at 4 °C. The high encapsulation efficiency for both chemical compounds ($EE_{MB} > 82\%$ and $EE_{CUR} > 90\%$) proved the bilosomes had a good capacity for MB and CUR co-encapsulation. It is worth noting that encapsulation of positively-charged MB did not significantly change the surface charge, thus proving its effective encapsulation in the aqueous core of the bilosome (excluding MB adsorption on the nanostructure surface). Functional polyphenol-loaded bilosomes with the hydrophilic photosensitizer Methylene Blue were also tested for fluorescence properties (Figure 1D). The presented emission spectrum under excitation with a wavelength of 666 nm (for MB) showed a slight blue shift in emission length for the encapsulated MB $\Delta_{\lambda MB} = 3$ nm, compared to the unencapsulated form of MB dissolved in distilled water.

Intermolecular Interaction Revealed by ATR-FTIR Spectroscopy

To complement spectroscopic experiments, we applied ATR-FTIR spectroscopy to verify the effectiveness of incorporating the two active compounds into the nanocarriers' structure. This method allowed us to provide wide-ranging information about the microenvironment of functional groups and, thus, to investigate the mechanisms of interaction of the encapsulated cargo with the bilosomes' structure. Accordingly, Figure 2 shows the spectra for empty bilosomes (grey line, Figure 2A), pure MB (blue line,

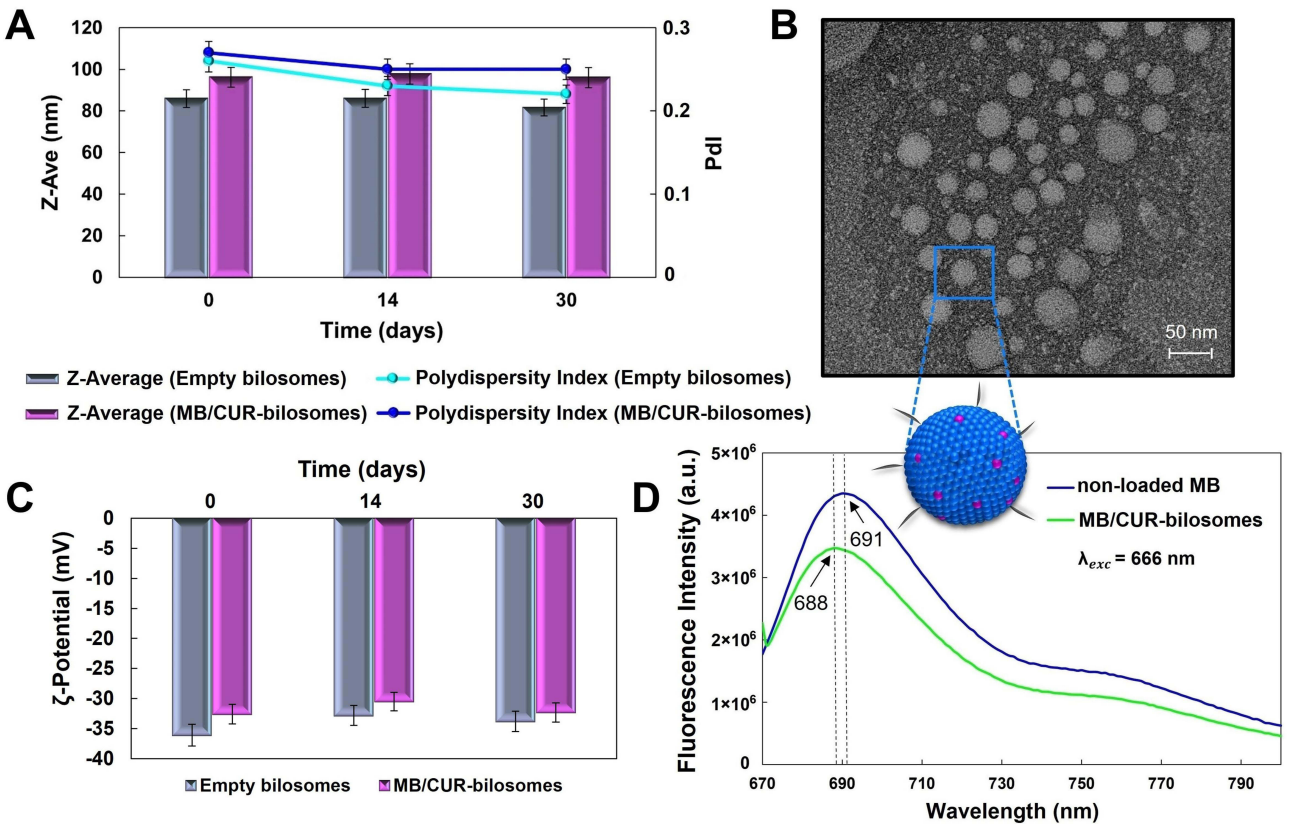

Figure 1 Physicochemical properties of bilosomal formulations. Effect of storage time on particle size (Z-Ave) and polydispersity index (PdI) for empty and MB/CUR-bilosomes (**A**). TEM image of MB/CUR-bilosomes. The scale bar represents 50 nm (**B**). Time-dependent colloidal stability of the empty and double-loaded bilosomes- ζ-Potential changes over time (**C**). Fluorescence emission spectra before and after MB encapsulation in functional bilosomes (λ_{exc}=666 nm) (**D**).

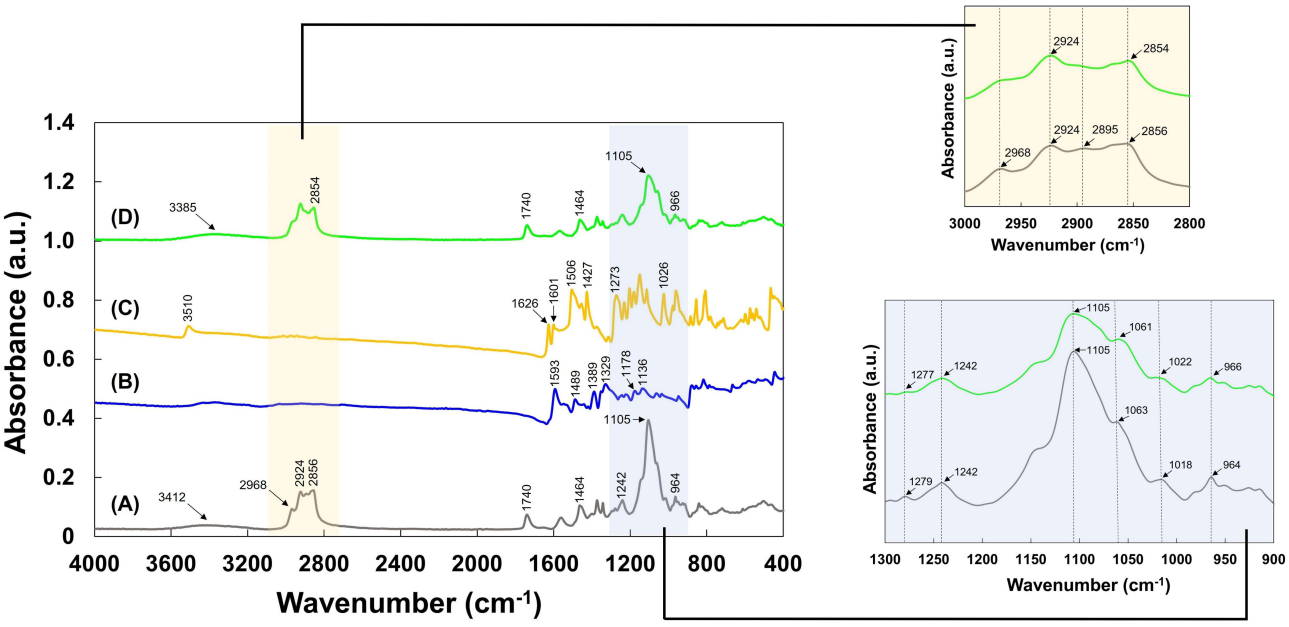

Figure 2 Comparative ATR-FTIR spectra for empty bilosomes (grey line, **A**), pure MB (blue line, **B**), pure CUR (yellow line, **C**), and MB/CUR-bilosomes (green line, **D**) in the whole range region (4000–400 cm^{-1} along with fingerprint regions of acyl chains (3000–2800 cm^{-1}) and polar head group (1300–900 cm^{-1}) of phospholipids for empty and double-loaded bilosomes.

Figure 2B), pure CUR (yellow line, Figure 2C), and MB/CUR-bilosomes (green line, Figure 2D) recorded over the entire range region (4000–400 cm^{-1}).

The FTIR spectrum of empty nanocarriers (Figure 2A) showed characteristic bands for phospholipid vesicles based on phosphatidylcholine, which is close to the results published by the other authors.[30,31] We can observe the stretching bands of CH_2 groups with maxima at 2924 cm^{-1} and 2856 cm^{-1}, which correspond to antisymmetric (ν^{as}_{CH}) and symmetric stretching (ν^{s}_{CH}) modes, respectively. Moreover, the band at 2968 cm^{-1} represents the antisymmetric stretching (ν^{as}_{CH}) of the terminal CH_3 groups. The minor but broad band from 3568 cm^{-1} to 3213 cm^{-1} (maximum at 3412 cm^{-1}) can be attributed to $v_{OH.O}$ stretching vibrations. There are related to the occurring hydrogen bonds between the bilosomal membranes and water molecules. The weak band assigned to the stretching vibration band of ester carbonyl groups (v_{co}) of the phospholipid appears at 1740 cm^{-1}. In addition, the peak at 1464 cm^{-1} represents the scissor vibrations (δ_{CH_2}) of CH_2 groups. Especially relevant (due to the sensitivity to structural changes) are the absorption bands originating from the polar part of the phospholipids located in the 1300–1000 cm^{-1} range. The maximum at 1242 cm^{-1} and the minor intensity band at 1279 cm^{-1} constitute antisymmetric PO^{2-} stretching vibrations (ν^{as}_{PO}). Meanwhile, the most intense band at 1105 cm^{-1} of the empty nanocarriers corresponds to symmetric PO^{2-} stretching vibrations (ν^{s}_{PO}). The band representing the choline antisymmetric stretching vibration of N^{+}-$(CH_3)_3$ (ν^{as}_{NC}) in the phosphatidylcholine head group was observed at 964 cm^{-1}.[32]

Several changes were noted in infrared absorption spectra after the encapsulation of MB and CUR in functional bilosomes (Figure 2D). We observed the most pronounced changes in the spectral area of the polar heads of phospholipids (1300–900 cm^{-1}). Comparing the MB/CUR-co-loaded bilosomes with empty nanocarriers, we observed a conspicuous decrease in band intensity at 1105 cm^{-1}, corresponding to symmetric PO^{2-} stretching vibrations (ν^{s}_{PO}). This situation proves the interaction of MB and CUR molecules with the hydrophilic part of the phospholipid. It can also be seen from the shift of the bands at 1279 cm^{-1} (ν^{as}_{PO}) and 1063 cm^{-1} (ν^{s}_{PO}) slightly toward the lower wavenumbers (1277 cm^{-1} and 1061 cm^{-1}, respectively), likely due to the hydrogen bond formation between PO^{2-} group and curcumin molecules containing hydroxyl groups.[33] It is also noticeable in the change of $v_{OH.O}$ position toward lower wavenumbers from 3412 cm^{-1} to 3385 cm^{-1}, which is related to the capacity to break hydrogen bonds and then form intermolecular hydrogen bonds among the phenolic OH groups derived from CUR and the phospholipids' functional groups (carboxyl and phosphate groups).[34] The fingerprint region for the polar head group of the lipid bilayer also shows a shift in the band characteristic of aliphatic phosphates (the P-O-C stretch), which changed from 1018 cm^{-1} to 1022 cm^{-1}. This shift was likely caused by the electrostatic interactions between sulfur present in the Methylene Blue structure, which has a positive charge, and the PC phosphate group.[35] The minor shift of N^{+}-$(CH_3)_3$ stretching vibrations toward higher wavenumbers (from 964 cm^{-1} to 966 cm^{-1}) was also observed (Figure 2).

It is worth noting that visible changes in the absorption bands corresponding to the acyl chains (3000–2800 cm^{-1}) were also observed after the active compounds were encapsulated in bilosomes. We noticed that the band at 2856 cm^{-1} shifted toward lower wavenumbers (2854 cm^{-1}). The red shift of absorption bands in the phospholipid's hydrophobic region after curcumin encapsulation indicates the presence of hydrophobic interactions between these components, which may correspond to a decrease in the mobility of the acyl chain and an increase in the ordering of the bilayer of the bilosomes.[34] In this region, we also observed a decreased intensity of the peak in the area corresponding to terminal CH_3 antisymmetric stretching vibration (2968 cm^{-1}) and terminal CH_3 symmetric stretching vibration (2895 cm^{-1}) for the double-loaded formulation, which means that the intensity of the absorption bands can depend on the packing density of the acyl chains. The band shifts after encapsulation of MB and CUR molecules in bilosomes suggest that they have been effectively encapsulated into the nanocarrier structure. FTIR spectra showed that the photosensitizer could therefore be bound to the bilosomes through electrostatic interactions with the polar part of the phospholipid. In the case of polyphenol, it is likely to have been incorporated inside the bilayer of the bilosomes through hydrophobic interactions with the phospholipid acyl chains or by forming hydrogen bonds with the hydrophilic head group present in the phospholipid structure. As shown in Figure 2, the resulting characteristic bands of pure MB (B) and pure CUR (C) vibrations (consistent with previous literature reports[36–39] disappeared after their incorporation into phospholipid vesicles, which also indicates their effective encapsulation.

Effect of Surface-Grafted PEG-Bilosomes on Protein Adsorption

Advances in the development of nanomaterials have resulted in many nanopharmaceuticals in clinical trials and various approved for clinical use.[40] Prominent among them are phospholipid vesicles (the so-called liposomes, as well as their modifications), which constitute a revolutionary nanocarrier showing beneficial aspects in the delivery of several drugs. However, there are some challenges affecting their efficacy, including, in particular, accelerated blood clearance, opsonization, uptake by the mononuclear phagocytic system (MPS) cells, inflammatory, allergic reactions, or even suppression of the immune system. One of the ways to improve the nanocarriers' physical and chemical properties, thereby preventing the adsorption of mediating serum proteins (called opsonins) that direct them to MPS for uptake and removal from the body, is to develop stealth nanoparticles due to minimal recognition by the human immune system. It can be achieved by coating the vesicle with polyethylene glycol (PEG), which creates a hydrophilic protective layer surrounding the nanocarrier with neutral electricity that increases the half-life of the particles in the blood circulation by several times through spatial repulsion.[41,42] Importantly, PEGylation not only sterically shields the nanoparticles, thus preventing their self-aggregation, adhesion of serum proteins to their surface, and ultimately removal by macrophages, but also reduces the toxicity of the drug molecules.[43]

The human immune system, as can be seen, is a multifactorial complex with which not only various receptors, inflammatory mediators, and cells are closely linked but also liposomal preparations introduced into the body. Therefore, these interactions must be considered to enable the nanocarriers to reach their target cells (including cancer cells). Accordingly, we conducted biological stability tests (Figure 3) in a physiological culture medium widely used for many cells (DMEM).

Stability tests were carried out both in DMEM without (Figure 3A) and supplemented with 10% FBS (Figure 3B). It was observed that the nanosystems' size distribution (an average diameter value from 91–99 nm) changed only marginally after adding biological fluid. In the case of medium without added FBS, the size of the carriers changed to 3 nm, while in the presence of 10% FBS only 6 nm, proving that the PEGylated surface induces inter-membrane repulsion and inhibits the aggregation of bilosomes (see Supplementary Table 1 for details). The results also indicated that the formed steric barrier between the bilosomal surface and the biological medium with the help of triblock copolymer (from the Pluronic family) resulted in protection against possible adsorption of serum proteins (including albumin, fibronectin, or IgG immunoglobulin). It is relevant because the opsonization of a nanocarrier gives it a new biological identity, after which it tends to affect specific tissues in different ways and has a significant role in immune recognition. Preventing the intermolecular aggregation process and nanocarriers' recognition by immune cells, leading successively to opsonization, followed by phagocytosis, determines effective and safe active cargo delivery to the target tissue.[44]

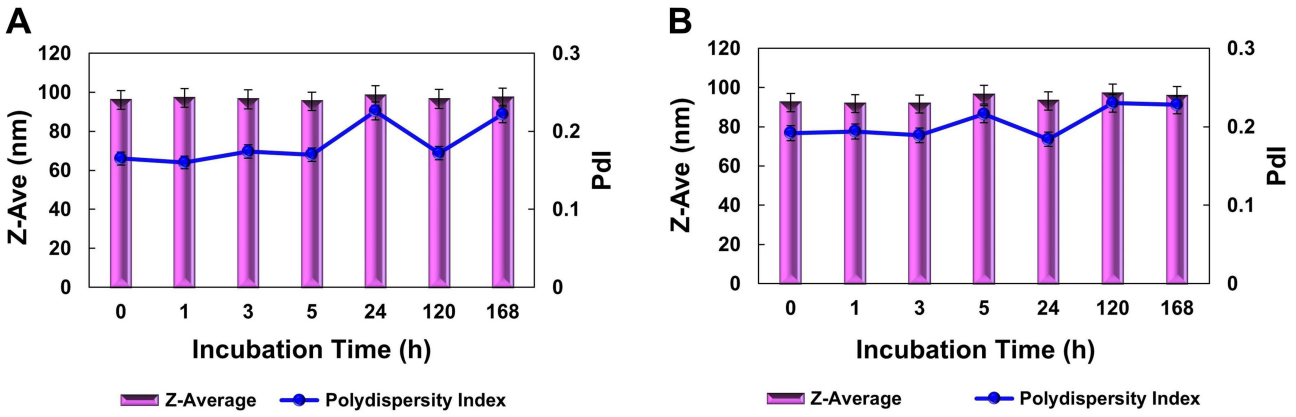

Figure 3 Distribution of Z-Average (Z-Ave) and polydispersity index (PdI) as a function of incubation time in DMEM without (**A**) and supplemented with 10% FBS (**B**) for MB/CUR-loaded bilosomes.

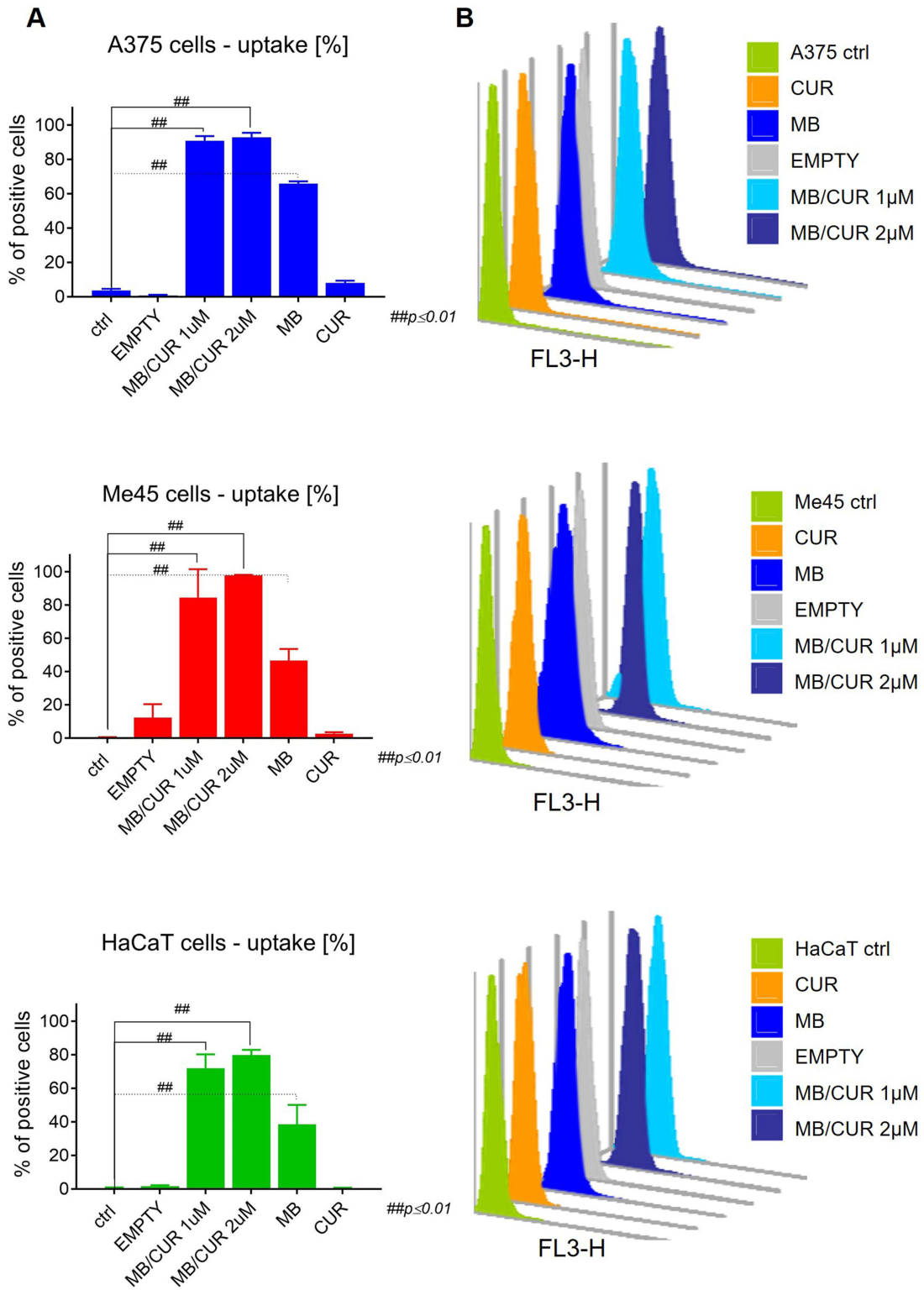

Figure 4 Flow cytometry uptake comparison of the studied nanosystems (**A**) by human cancer A375, Me45, and normal HaCaT cell lines with the corresponding histograms (**B**) after 24 h incubation at 37 °C, ##Statistical analysis: $p \leq 0.01$.

Quantitative Evaluation of the Hybrid Bilosomes Internalization Capacity

Figure 4 shows the percentage of positive cells for uptake of free and encapsulated MB and CUR in bilosomes across three cell lines: A375 (blue), Me45 (red), and HaCaT (green). Control groups (ctrl) are present for each cell line. The

empty nanocarriers were applied as a negative control and did not cause uptake. The hybrid bilosome was tested at two concentrations - 1 μM and 2 μM (related to the final MB concentration). In the case of A375 cells, both 1 μM and 2 μM concentrations of MB/CUR-loaded bilosomes show a high percentage of positive cells, with the effect appearing slightly dose-dependent as there's a reduction in uptake at 1 μM compared to 2 μM. The same pattern is observed for the Me45 cell line, although the percentage of positive cells is higher compared to the A375 for both concentrations of the hybrid bilosomes. In the case of the healthy HaCaT cell line, MB/CUR-loaded bilosomes revealed a decreased uptake comparable to both cancer cells, indicating some selectivity upon the normal skin cell lines. The MB alone shows minimal uptake in all three cell lines, with the A375 and Me45 having almost negligible positive cells and HaCaT having a higher percentage but still much lower in contrast to the loaded nanocarrier treatments. The CUR alone reveals a non-significant response with low uptake in all used cell lines. Statistical analysis confirmed that the differences in cargo uptake were significant ($p \leq 0.01$) compared to the control within each cell line.

Bioimaging and Immunofluorescence Study

Bioimaging results are shown in Figure 5. We investigated the effects of bilosomes, empty ones, and drug-loaded on cellular morphology. Firstly we provided 3D cell bioimaging using holotomographic microscopy (HTM), which demonstrated cellular morphology with stained nuclei post-exposure to bilosomes or free active cargo (Figure 5A).

Interestingly, exposure to bilosomes did not cause any observable changes in cellular morphology (Figure 5). However, when cells were exposed to free drugs MB (Methylene Blue) or CUR (curcumin), a notable reduction in cell number was observed. Additionally, CUR exposure induced a slight elongation of the cell shape in the case of Me45

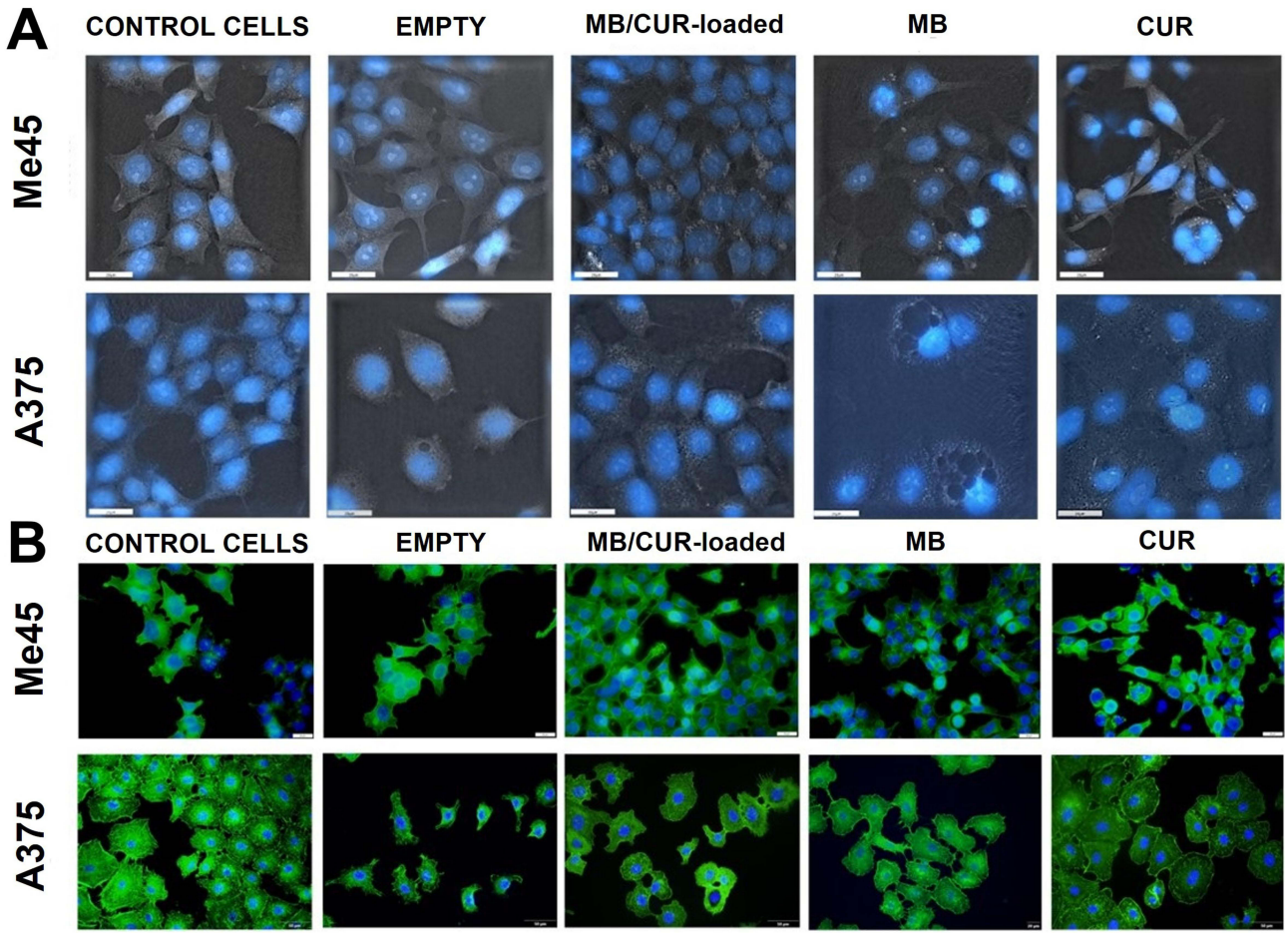

Figure 5 Bioimaging and immunofluorescence study in Me45 and A375 cells (the final PS concentration was 2 μM). Holotomographic-HTM-visualization of the human melanoma morphology (**A**), immunofluorescent F-actin staining (**B**) of Me45 and A375 cells.

cells. Analyzing the A375 morphology, we could observe a significant cytoplasmic vacuolization after treatment with free MB. It might be a symptom of caspase-independent cell death, including paraptosis or methuosis.[45] In both cell lines, the exposition to MB/CUR-bilosomes provoked an accumulation of lysosomes, that is, lysosomal stress response (LSR). LSR is also an early marker of autophagy, and whether the cell dies or is restored to homeostasis depends on the intensity of this stress.[46] To further analyze the impact of drug exposure on cellular structures, we conducted F-actin staining to visualize the cellular cytoskeleton (Figure 5B). There was not observed a significant reorganization of actin fibers upon exposure to bilosomes, indicating that these nanostructures did not influence the cytoskeletal dynamics. Similarly to HTM imaging, in the case of Me45 (Figure 5A), we also observed the elongation of the cells and a noticeable tension of the stress fibers after exposure to CUR alone. These findings shed light on the biocompatibility of bilosomes, which appear to have no direct impact on cellular morphology or actin cytoskeleton dynamics, which correspond to safety profiles in biomedical applications.

Cytocompatibility and Phyto-Photodynamic Activity

In the next step of our research, we assessed the cytocompatibility of the created bilosomes upon human skin melanoma cells. For this purpose, a human melanoma cell line derived from the explant culture of a 54-year-old woman's solid tumor (A375) and a malignant tumor derived from lymph node metastases of cutaneous melanoma (Me45) were used. Accordingly, the cytotoxicity of empty and MB/CUR-loaded bilosomes expressed in terms of mitochondrial dehydrogenase activity (MTT cell proliferation assay) was examined at different concentrations of MB (from 0.5 μM to 12.5 μM). The viability studies, which were estimated after incubation in the dark condition for 24 hours of the bilosome formulation tested (Supplementary Figure 1), showed the safety of bilosomes from a concentration of 2 μM (for the A375 cell line, as well as Me45). Furthermore, for additional incubation time up to 72 hours, we observed regeneration of the mitochondrial activity and a significant increase in A375 cell viability over the entire concentration range tested, even for the highest 12.5 μM, reaching more than 80% of control cells. Unfortunately, for the Me45 cell line (after a 72-hour incubation), the opposite effect and a decrease in the mitochondrial dehydrogenase activity followed by a significant reduction in the cell viability were noted. This phenomenon could be explained as a result of the LSR observed during the HTM bioimaging. For the A375 cells, the level of lysosomal stress might not have reached a critical threshold within the initial 72 hours, thus avoiding triggering the cell death pathway. Instead, the cells might have exhibited a multifaceted response. First, these cells could have initiated a set of protective mechanisms aimed at mitigating the effects of lysosomal stress. This might involve upregulation of lysosomal biogenesis, activation of autophagic pathways to clear damaged organelles, and engagement of anti-oxidative defenses to counteract the stress-induced reactive oxygen species.[47] A375 cells could have succeeded in gradually alleviating the initial lysosomal stress and transitioning towards a state of cellular homeostasis. As a result, the screening study allowed us to choose the most favorable incubation time and dilution of the bilosomal sample, ultimately equal to the final concentration of 2 μM loaded MB for the following phyto-photodynamic activity. However, before evaluating the bilosomes photocytotoxicity, the cytocompatibility of the selected formulation was also checked upon primary human cutaneous keratinocytes (HaCaT), applied as a normal cell line. The incubation time-dependent cytotoxicity of the optimal concentration of the nanoplatform, shown in Supplementary Figure 2, proved its safety upon human normal skin cells, even though some uptake of the tested carriers was observed in flow cytometry experiments. Furthermore, the protective effect of bilosomes on the active cargo, even after an extended incubation time of up to 72 hours, was observed, indicating significant mitochondria regeneration and proving that the studied formulations do not change the HaCaT culture metabolic conditions. Atrux-Tallau et al[48] also demonstrated a time-dependent increase in human keratinocyte cell viability after incubation with other phospholipid-based nanocarriers. The observed phenomenon may be due to the beneficial effect of phospholipids on the proliferation of the HaCaT cell line so that the obtained bilosomes can be considered non-cytotoxic to the HaCaT cell line even compared to other nanocarriers reported in the literature and tested in skin application studies.[28] The substantial goal of this study was the efficacy of phyto-PDT hybrid bilosomes. As shown in Figure 6, exposure of melanoma cancer cells to red light followed by 24-hour incubation with MB/CUR-bilosomes significantly reduced mitochondrial activity, leading to less dehydrogenase activity and resulting in fewer remaining viable cells in both A375 and Me45 cell lines compared to free PS molecules. Moreover, the high photoactivity of the dye (after encapsulation in the nanostructures) may be

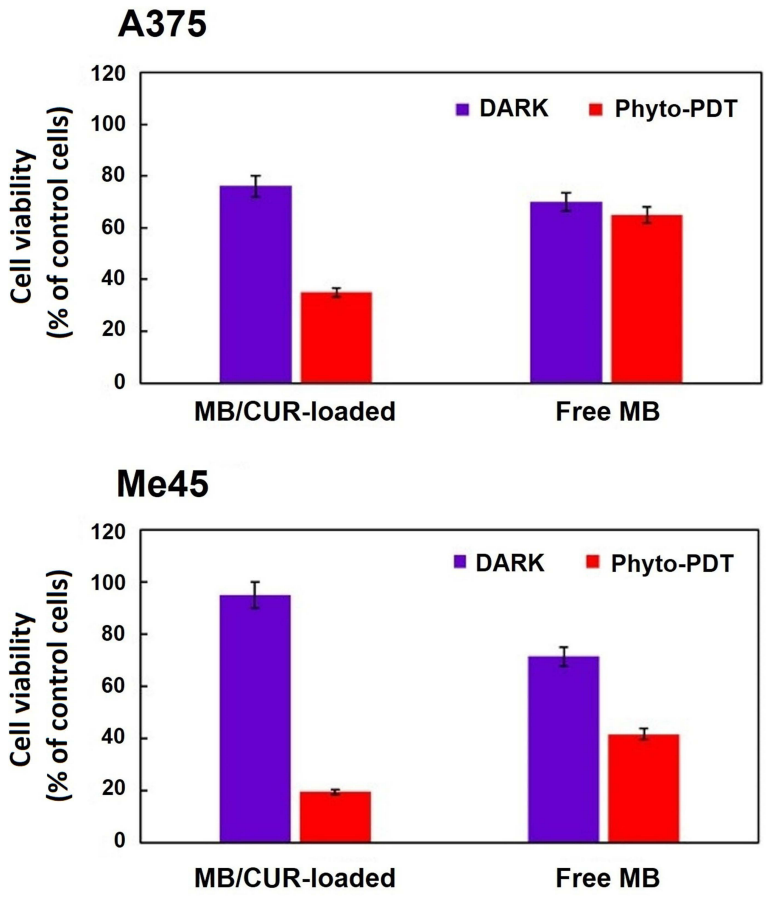

Figure 6 The dark cytotoxicity (without irradiation) and photocytotoxicity (phyto-PDT action) of the MB/CUR-loaded bilosomes compared to the free MB molecules (the final PS concentration was 2 μM), upon human melanoma A375 and Me45 cell lines, after incubation for 24 h post red light irradiation.

responsible for the higher efficacy of double-loaded bilosomes in PDT therapy. The unencapsulated MB has an intense tendency to aggregate in aqueous solutions, complicating the ability to produce singlet oxygen. The MB aggregates formed then tend toward electron transfer reactions instead of energy transfer with oxygen, ultimately reducing the effectiveness of the free molecule in the photodynamic therapy.[49] Thus, encapsulating the hydrophilic photosensitizer in advanced bilosomes prevents its rapid photobleaching, which was confirmed in our previous studies.[22] Studies on cell lines also showed a photocytotoxic effect was found to be more significant upon Me45 cells (decrease in the cell viability index less than 20% of control) compared to the A375 cell line (decrease in the cell viability index less than 35% of control). The obtained results may be also caused by the improved uptake of the encapsulated cargo upon Me45 cells as was demonstrated above in flow cytometry experiments.

Our results indicate that bilosomal based nanosystems are more effective in metastatic cells. Metastatic cells, are known to be highly mobile and invasive,[50] so effective targeting becomes crucial. This might be promising in the case of the advanced staged or secondary treatment of melanoma, where selective approaches are required. Bilosomes are stable nanosystems whose extended circulation time increases the chances of encountering metastatic cells and improves drug delivery to distant sites. In addition, the use of bilosomes can also protect cargo, which is particularly important in photodynamic procedures.[21,22] These encouraging results demonstrate the potential application of the bilosomal MB/CUR nanoplatform for skin melanoma constitutes and further in vivo studies.

Conclusion

In the following paper, we demonstrated the biological capacity of the novel hybrid transdermal nanoplatform upon skin melanoma cell lines, including human epithelial skin melanoma A375 cells and human malignant melanoma Me45 cell line. The

hybrid bilosomes co-stabilized by biocompatible building blocks (phospholipids, bile salts, cholesterol, and polymeric triblock materials) demonstrated good capacity for the co-encapsulation of classical photosensitizer (Methylene Blue, MB) along with a complementary natural polyphenolic compound (curcumin, CUR). The nanoscopic size (D_H < 100 nm) and negative surface charge (ζ < - 37 mV) of the nanoplatform were revealed in DLS and ELS measurements, while its spherical morphology was by TEM imaging. Research using UV-Vis, ATR-FTIR, and fluorescent spectroscopies confirmed the improved incorporation and stability of the co-loaded hybrid cargo into the bilosome structure. The colloidal stability tests carried out in biological fluids (both in DMEM containing 10% FBS and without the addition of FBS) proved the protective effect of the PEGylated surface upon the nanocarrier aggregation and simultaneously a steric barrier between the bilosomal surface and the biological medium resulted in protection against possible adsorption of serum proteins. Bioimaging and immunofluorescence study revealed no significant impact of empty or loaded bilosomes on melanoma cells contrary to the free active cargo (MB or CUR alone) forms when we observed a notable reduction in cell number or other significant morphological changes. Furthermore, the in vitro cytotoxicity studies on normal keratinocytes and non-irradiated cancer cells showed the protective effect of the nanoplatform shield co-loaded by the hybrid cargo. Although phyto-PDT action after red-light irradiation confirmed a decrease in mitochondrial activity, primarily upon Me45 cells (decrease in the cell viability index below 20% relative to the control), proving the potential of newly designed bilosomes as biocompatible and comprehensive nanoplatform for further melanoma cancer investigations.

Abbreviations

PDT, photodynamic therapy; FDA, Food and Drug Administration; ROS, reactive oxygen species; PSs, photosensitizers; EMT, epithelial-mesenchymal transition; MAPK, mitogen-activated protein kinase; EPR, enhanced permeability and retention; MB, Methylene Blue; CUR, curcumin; HTM, holotomographic microscopy; FM, fluorescence microscopy; A375, human epithelial skin melanoma cell line; Me45, human malignant melanoma cell line; phyto-PDT, phyto-photodynamic therapy; PC, phosphatidylcholine; SC, sodium cholate; PP123, Pluronic®P123; Chol, cholesterol; THF, tetrahydrofuran; SUVs, small unilamellar vesicles; DLS, dynamic light scattering; ELS, electrophoretic light scattering; Z-Ave, Z-Average; PdI, polydispersity index; TEM, transmission electron microscopy; EE, encapsulation efficiency; ATR-FTIR, attenuated total reflection-Fourier transform infrared spectroscopy; DMEM, Dulbecco's Modified Eagle's Medium; FBS, fetal bovine serum; HaCaT, human keratinocyte cell line; DPBS, Dulbecco's Phosphate Buffered Saline; DAPI, 4.6-diamidino-2-phenylindole; MTT, 3-(4,5-dimethylthiazol-2-yl)-2,5-diphenyl tetrazolium bromide; GIT, gastro-intestinal tract; MPS, mononuclear phagocytic system; PEG, polyethylene glycol; LSR, lysosomal stress response.

Acknowledgments

The support from the Department of Physical and Quantum Chemistry at Wroclaw University of Science and Technology and partially by the Statutory Subsidy Funds of the Department of Molecular and Cellular Biology no. SUBZ. D260.24.076 at Wroclaw Medical University is gratefully acknowledged.

Disclosure

The authors of this paper declare no competing financial or other interests that could affect the work they describe here.

References

1. Wang T, Xu P, Fang J, et al. Synthesis and preclinical evaluation of a ^{68}Ga-labeled pyridine-based benzamide dimer for malignant melanoma imaging. *Mol Pharm*. 2023;20(2):1015–1024. doi:10.1021/acs.molpharmaceut.2c00745
2. Rahimi A, Esmaeili Y, Dana N, et al. A comprehensive review on novel targeted therapy methods and nanotechnology-based gene delivery systems in melanoma. *Eur J Pharm Sci*. 2023;187:106476. doi:10.1016/j.ejps.2023.106476
3. Fan L, Wang Z, Shi D. Targeted nanoscale drug delivery systems for melanoma therapy. *J Drug Deliv Sci Technol*. 2023;86:104724. doi:10.1016/j.jddst.2023.104724
4. Jiang T, Wang T, Li T, et al. Enhanced transdermal drug delivery by transfersome-embedded oligopeptide hydrogel for topical chemotherapy of melanoma. *ACS Nano*. 2018;12(10):9693–9701. doi:10.1021/acsnano.8b03800
5. Wang J, Liao H, Ban J, et al. Multifunctional near-infrared dye IR-817 encapsulated in albumin nanoparticles for enhanced imaging and photothermal therapy in melanoma. *Int J Nanomed*. 2023;18:4949–4967. doi:10.2147/IJN.S425013
6. Bazylinska U, Kulbacka J, Schmidt J, et al. Polymer-free cubosomes for simultaneous bioimaging and photodynamic action of photosensitizers in melanoma skin cancer cells. *J Colloid Interface Sci*. 2018;522:163–173. doi:10.1016/j.jcis.2018.03.063

7. Gunaydin G, Gedik ME, Ayan S. Photodynamic therapy for the treatment and diagnosis of cancer – a review of the current clinical status. *Front Chem*. 2021;9:686303. doi:10.3389/fchem.2021.686303
8. Zhou J, Liu C, Wang Y, et al. Prodrug and glucose oxidase coloaded photodynamic hydrogels for combinational therapy of melanoma. *ACS Biomater Sci Eng*. 2022;8(11):4886–4895. doi:10.1021/acsbiomaterials.2c00992
9. Szlasa W, Supplitt S, Drąg-Zalesinska M, et al. Effects of curcumin based PDT on the viability and the organization of actin in melanotic (A375) and amelanotic melanoma (C32)–*in vitro* studies. *Biomed Pharmacother*. 2020;132:110883. doi:10.1016/j.biopha.2020.110883
10. Li XY, Tan LC, Dong LW, et al. Susceptibility and resistance mechanisms during photodynamic therapy of melanoma. *Front Oncol*. 2020;10:597. doi:10.3389/fonc.2020.00597
11. Wang L, Wang L, Zhang Y, et al. LS-HB-mediated photodynamic therapy inhibits proliferation and induces cell apoptosis in melanoma. *Mol Pharm*. 2022;19(7):2607–2619. doi:10.1021/acs.molpharmaceut.2c00302
12. Jung E, Shim I, An J, et al. Phenylthiourea-conjugated BODIPY as an efficient photosensitizer for tyrosinase-positive melanoma-targeted photodynamic therapy. *ACS Appl Bio Mater*. 2021;4(3):2120–2127. doi:10.1021/acsabm.0c01322
13. Zhang W, Du XF, Liu B, et al. Engineering supramolecular nanomedicine for targeted near infrared-triggered mitochondrial dysfunction to potentiate cisplatin for efficient chemophototherapy. *ACS Nano*. 2022;16(1):1421–1435. doi:10.1021/acsnano.1c09555
14. Lara-Vega I, Vega-Lopez A. Combinational photodynamic and photothermal-based therapies for melanoma in mouse models. *Photodiagnosis Photodyn Ther*. 2023;43:103596. doi:10.1016/j.pdpdt.2023.103596
15. Ng CY, Yen H, Hsiao HY, Su SC. Phytochemicals in skin cancer prevention and treatment: an updated review. *Int J Mol Sci*. 2018;19(4):941. doi:10.3390/ijms19040941
16. Chen X, Yi Z, Chen G, et al. Carrier-enhanced photodynamic cancer therapy of self-assembled green tea polyphenol-based nanoformulations. *ACS Sustain. Chem Eng*. 2020;8(43):16372–16384. doi:10.1021/acssuschemeng.0c06645
17. Mardani R, Hamblin MR, Taghizadeh M, et al. Nanomicellar-curcumin exerts its therapeutic effects via affecting angiogenesis, apoptosis, and T cells in a mouse model of melanoma lung metastasis. *Pathol Res Pract*. 2020;216:153082. doi:10.1016/j.prp.2020.153082
18. Lelli D, Pedone C, Sahebkar A. Curcumin and treatment of melanoma: the potential role of microRNAs. *Biomed Pharmacoth*. 2017;88:832–834. doi:10.1016/j.biopha.2017.01.078
19. Meng J, Guo F, Xu H, et al. Combination therapy using co-encapsulated resveratrol and paclitaxel in liposomes for drug resistance reversal in breast cancer cells *in vivo*. *Sci Rep*. 2016;6:22390. doi:10.1038/srep22390
20. Wi TI, Won JE, Lee CM, et al. Efficacy of combination therapy with linalool and doxorubicin encapsulated by liposomes as a two-in-one hybrid carrier system for epithelial ovarian carcinoma. *Int J Nanomed*. 2020;15:8427–8436. doi:10.2147/IJN.S272319
21. Waglewska E, Pucek-Kaczmarek A, Bazylinska U. Self-assembled bilosomes with stimuli-responsive properties as bioinspired dual-tunable nanoplatform for pH/temperature-triggered release of hybrid cargo. *Colloids Surf B*. 2022;215:112524. doi:10.1016/j.colsurfb.2022.112524
22. Waglewska E, Maliszewska I, Bazylinska U. Antimicrobial phyto-photodynamic activity inducing by polyphenol-supported Methylene Blue co-loaded into multifunctional bilosomes: advanced hybrid nanoplatform in the skin infections treatment? *J Photochem Photobiol B: Biol*. 2023;240:112650. doi:10.1016/j.jphotobiol.2023.112650
23. Baskaran R, Lee J, Yang SG. Clinical development of photodynamic agents and therapeutic applications. *Biomater Res*. 2018;22:25. doi:10.1186/s40824-018-0140-z
24. Münch S, Wohlrab J, Neubert RHH. Dermal and transdermal delivery of pharmaceutically relevant macromolecules. *Eur J Pharm Biopharm*. 2017;119:235–242. doi:10.1016/j.ejpb.2017.06.019
25. Pucek A, Tokarek B, Waglewska E, Bazylinska U. Recent advances in the structural design of photosensitive agent formulations using "soft" colloidal nanocarriers. *Pharmaceutics*. 2020;12(6):587. doi:10.3390/pharmaceutics12060587
26. Sala M, Diab R, Elaissari A, Fessi H. Lipid nanocarriers as skin drug delivery systems: properties, mechanisms of skin interactions and medical applications. *Int J Pharm*. 2018;535(1–2):1–17. doi:10.1016/j.ijpharm.2017.10.046
27. Ahmed S, Kassem MA, Sayed S. Bilosomes as promising nanovesicular carriers for improved transdermal delivery: construction, *in vitro* optimization, *ex vivo* permeation and *in vivo* evaluation. *Int J Nanomed*. 2020;15:9783–9798. doi:10.2147/IJN.S278688
28. Cai X, Jin M, Yao L, et al. Physicochemical properties, pharmacokinetics, toxicology and application of nanocarriers. *J Mater Chem B*. 2023;11:716–733. doi:10.1039/d2tb02001g
29. Sheikholeslami B, Lam NW, Dua K, Haghi M. Exploring the impact of physicochemical properties of liposomal formulations on their *in vivo* fate. *Life Sci*. 2022;300:120574. doi:10.1016/j.lfs.2022.120574
30. Elkholy NS, Shafaa MW, Mohammed HS. Biophysical characterization of lutein or beta carotene-loaded cationic liposomes. *RSC Adv*. 2020;10:32409–32422. doi:10.1039/d0ra05683a
31. Pawlikowska-Pawlega B, Misiak LE, Zarzyka B, et al. FTIR, ^{1}H NMR and EPR spectroscopy studies on the interaction of flavone apigenin with dipalmitoylphosphatidylcholine liposomes. *Biochim Biophys Acta - Biomembr*. 2013;1828(2):518–527. doi:10.1016/j.bbamem.2012.10.013
32. Chen C, Tripp CP. An infrared spectroscopic based method to measure membrane permeance in liposomes. *Biochimica et Biophysica Acta (BBA) - Biomembranes*. 2008;1778(10):2266–2272. doi:10.1016/j.bbamem.2008.05.010
33. Tai K, Rappolt M, Mao L, et al. Stability and release performance of curcumin-loaded liposomes with varying content of hydrogenated phospholipids. *Food Chem*. 2020;326:126973. doi:10.1016/j.foodchem.2020.126973
34. Hasan M, Ben Messaoud G, Michaux F, et al. Chitosan-coated liposomes encapsulating curcumin: study of lipid-polysaccharide interactions and nanovesicle behavior. *RSC Adv*. 2016;6:45290–45304. doi:10.1039/c6ra05574e
35. Maximino MD, Constantino CJL, Oliveira ON, Alessio P. Synergy in the interaction of amoxicillin and methylene blue with dipalmitoyl phosphatidyl choline (DPPC) monolayers. *Appl Surf Sci*. 2019;476:493–500. doi:10.1016/j.apsusc.2019.01.065
36. Liu B, Wen L, Nakata K, et al. Polymeric adsorption of methylene blue in TiO_2 colloids-highly sensitive thermochromism and selective photocatalysis. *Chem - a Eur J*. 2012;18(40):12705–12711. doi:10.1002/chem.201200178
37. Farmoudeh A, Akbari J, Saeedi M, et al. Methylene blue-loaded niosome: preparation, physicochemical characterization, and *in vivo* wound healing assessment. *Drug Delivery Trans Res*. 2020;10(5):1428–1441. doi:10.1007/s13346-020-00715-6
38. Yang -Q-Q, Cai W-Q, Z.-x W, et al. Structural characteristics, binding behaviors, and stability of ternary nanocomplexes of lecithin, polyvinylpyrrolidone, and curcumin. *Lwt*. 2023;175:114489. doi:10.1016/j.lwt.2023.114489

39. Lai D, Zhou A, Tan BK, et al. Preparation and photodynamic bactericidal effects of curcumin-β-cyclodextrin complex. *Food Chem*. 2021;361:130117. doi:10.1016/j.foodchem.2021.130117
40. Vu VP, Gifford GB, Chen F, et al. Immunoglobulin deposition on biomolecule Corona determines complement opsonization efficiency of preclinical and clinical nanoparticles. *Nat Nanotechnol*. 2019;14(3):260–268. doi:10.1038/s41565-018-0344-3
41. Shi L, Zhang J, Zhao M, et al. Effects of polyethylene glycol on the surface of nanoparticles for targeted drug delivery. *Nanoscale*. 2021;13:10748–10764. doi:10.1039/d1nr02065j
42. Bazylinska U. Rationally designed double emulsion process for co-encapsulation of hybrid cargo in stealth nanocarriers. *Colloids Surf A Physicochem Eng Aspects*. 2017;532:476–482. doi:10.1016/j.colsurfa.2017.04.027
43. Lee H, Larson RG. Adsorption of plasma proteins onto PEGylated lipid bilayers: the effect of PEG size and grafting density. *Biomacromolecules*. 2016;17(5):1757–1765. doi:10.1021/acs.biomac.6b00146
44. Zahednezhad F, Saadat M, Valizadeh H, et al. Liposome and immune system interplay: challenges and potentials. *J Control Release*. 2019;305:194–209. doi:10.1016/j.jconrel.2019.05.030
45. Hanson S, Dharan A, J PV, et al. Paraptosis: a unique cell death mode for targeting cancer. *Front Pharmacol*. 2023;14:1159409. doi:10.3389/fphar.2023.1159409
46. Lakpa KL, Khan N, Afghah Z, et al. Lysosomal stress response (LSR): physiological importance and pathological relevance. *J Neuroimmune Pharmacol*. 2021;16(2):219–237. doi:10.1007/s11481-021-09990-7
47. Filomeni G, De Zio D, Cecconi F. Oxidative stress and autophagy: the clash between damage and metabolic needs. *Cell Death Differ*. 2015;22(3):377–388. doi:10.1038/cdd.2014.150
48. Atrux-Tallau N, Delmas T, Han SH, et al. Skin cell targeting with self-assembled ligand addressed nanoemulsion droplets. *Int J Cosmet Sci*. 2013;35(3):310–318. doi:10.1111/ics.12044
49. Nunez SC, Yoshimura TM, Ribeiro MS, et al. Urea enhances the photodynamic efficiency of methylene blue. *J Photochem Photobiol B: Biol*. 2015;150:31–37. doi:10.1016/j.jphotobiol.2015.03.018
50. Fares J, Fares MY, Khachfe HH, et al. Molecular principles of metastasis: a hallmark of cancer revisited. *Signal Transduct Target Ther*. 2020;5:28. doi:10.1038/s41392-020-0134-x